Nucleic Acids Research, 2024, 1–15
https://doi.org/10.1093/nar/gkae177
RNA and RNA-protein complexes

Substrate specificity of *Mycobacterium tuberculosis* tRNA terminal nucleotidyltransferase toxin MenT3

Jun Liu[1], Yuka Yashiro[1], Yuriko Sakaguchi[2], Tsutomu Suzuki[2] and Kozo Tomita[1,*]

[1]Department of Computational Biology and Medical Sciences, Graduate School of Frontier Sciences, The University of Tokyo, Kashiwa, Chiba 277-8562, Japan
[2]Department of Chemistry and Biotechnology, Graduate School of Engineering, The University of Tokyo, Bunkyo-ku, Tokyo 113-8656, Japan
[*]To whom correspondence should be addressed. Tel: +81 471363611; Email: kozo-tomita@edu.k.u-tokyo.ac.jp

Abstract

Mycobacterium tuberculosis transfer RNA (tRNA) terminal nucleotidyltransferase toxin, MenT3, incorporates nucleotides at the 3′-CCA end of tRNAs, blocking their aminoacylation and inhibiting protein synthesis. Here, we show that MenT3 most effectively adds CMPs to the 3′-CCA end of tRNA. The crystal structure of MenT3 in complex with CTP reveals a CTP-specific nucleotide-binding pocket. The 4-NH_2 and the N_3 and O_2 atoms of cytosine in CTP form hydrogen bonds with the main-chain carbonyl oxygen of P120 and the side chain of R238, respectively. MenT3 expression in *Escherichia coli* selectively reduces the levels of seryl-tRNA^{Ser}s, indicating specific inactivation of tRNA^{Ser}s by MenT3. Consistently, MenT3 incorporates CMPs into tRNA^{Ser} most efficiently, among the tested *E. coli* tRNA species. The longer variable loop unique to class II tRNA^{Ser}s is crucial for efficient CMP incorporation into tRNA^{Ser} by MenT3. Replacing the variable loop of *E. coli* tRNA^{Ala} with the longer variable loop of *M. tuberculosis* tRNA^{Ser} enables MenT3 to incorporate CMPs into the chimeric tRNA^{Ala}. The N-terminal positively charged region of MenT3 is required for CMP incorporation into tRNA^{Ser}. A docking model of tRNA onto MenT3 suggests that an interaction between the N-terminal region and the longer variable loop of tRNA^{Ser} facilitates tRNA substrate selection.

Graphical abstract

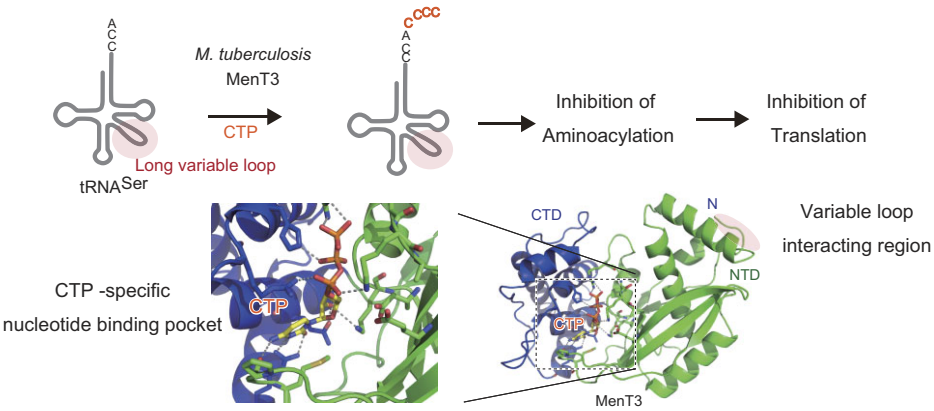

Introduction

Bacterial toxin–antitoxin (TA) systems are essential for bacterial growth and survival under various conditions (1–4). The bacterial TA module consists of a gene pair, encoding a toxin and an antitoxin, within an operon. Protein toxins of the bacterial TA modules impede crucial cellular biological processes, including DNA replication, transcription, protein synthesis and cell wall synthesis, thereby regulating bacterial growth (2). Under normal physiological conditions, antitoxins, either RNAs or proteins, neutralize toxin activities by suppressing toxin expression or activity. During environmental stresses, such as nutrient starvation, the protein or RNA antitoxins are degraded or downregulated. As a result, the repression of toxin expression or activity is released, leading bacteria to stop their own growth (2,5–7).

The TA systems were previously categorized into six classes (types I–VI), based on the antitoxin properties and the modes of toxin activity and expression neutralization (7,8). Recently, new types of TA systems have been identified, expanding the number of TA system classes to eight (types I–VIII) (9,10). In the type VII TA system, the protein antitoxins are enzymes that modify the cognate toxins, thereby neutralizing/repressing the toxin activity (11–14) or reducing the stability of the toxin proteins (15).

Members of the MenAT family of TA systems in the human pathogen *Mycobacterium tuberculosis* encode a toxin with a

Received: December 25, 2023. **Revised:** February 13, 2024. **Editorial Decision:** February 21, 2024. **Accepted:** February 28, 2024

conserved nucleotidyltransferase-like domain and a cognate antitoxin (16). Among the four members of the MenAT family, the MenT1, MenT3 and MenT4 toxins function as transfer RNA (tRNA) nucleotidyltransferase toxins, adding nucleotides onto the 3′-CCA end of tRNAs *in vitro* (16,17). These extra nucleotides block the aminoacylation of tRNAs by aminoacyl-tRNA (aa-tRNA) synthetase, leading to the inhibition of protein synthesis.

MenAT1 belongs to the type II TA system, and the MenT1 activity is inhibited by the antitoxin MenA1 through its asymmetrical binding to MenT1 (17). In contrast, MenAT3 and possibly MenAT4 belong to the type VII TA system. The antitoxin MenA3 reportedly functions as an atypical serine protein kinase, phosphorylating Ser78 close to the active site in MenT3. Thus, MenA3 inactivates MenT3 through phosphomodification (14). MenA4 apparently has a C-terminal kinase domain similar to MenA3 (18); thus, MenA4 may also neutralize/suppress the MenT4 activity through the phosphorylation of the corresponding serine residue close to its active site.

In vitro, MenT1 incorporated CMPs onto the 3′-CCA end of tRNA without tRNA preferences (17). MenT3 added pyrimidines (CMPs or UMPs) onto the 3′-CCA end of several tRNA species, with preference for the $tRNA^{Ser}$ isoacceptor *in vitro* (16). Conversely, MenT4 incorporated GMP onto the 3′-CCA end of tRNAs without preferences *in vitro* (17). Thus, the substrate specificities of the MenT tRNA nucleotidyltransferase toxins are diverse, and their specific molecular mechanisms have remained elusive.

Here, we present functional and structural analyses of MenT3. We show that MenT3 efficiently incorporates CMP onto the 3′-CCA of tRNAs. The crystal structure of MenT3 in complex with CTP revealed the molecular basis of its nucleotide specificity. We also show that MenT3 specifically reduced the level of seryl-$tRNA^{Ser}$s when expressed in *Escherichia coli*. The longer variable loop of substrate $tRNA^{Ser}$ is required for CMP incorporation onto $tRNA^{Ser}$ isoacceptors. A tRNA docking model suggests that the N-terminal positively charged region of MenT3 interacts with the variable loop of $tRNA^{Ser}$, thereby selecting the substrate tRNA. Altogether, MenT3 is a CTP:tRNA nucleotidyltransferase toxin targeting $tRNA^{Ser}$ isoacceptors. The possible mechanisms underlying the different substrate specificities of the MenT tRNA nucleotidyltransferase toxins are discussed.

Materials and methods

Plasmid construction

Synthetic DNA encoding the *MenA3–MenT3* module (14,16) from *M. tuberculosis* was purchased from Eurofins, Japan. The nucleotide sequence of the *MenA3–MenT3* module is provided in Supplementary Table S1. For overexpression of wild-type MenT3 in *E. coli*, the *MenT3* gene was PCR (polymerase chain reaction) amplified and cloned between the NdeI and XhoI sites of pET22b (Novagen), yielding pET22-MenT3. To generate plasmids for the expression of the catalytically inactive MenT3(D80A) mutant protein, synthetic DNA encoding the MenT3(D80A) was cloned between the NdeI and XhoI sites of pET22b, yielding the plasmid pET22-MenT3_D80A. pET22-MenT3 variants with a mutation in the MenT3 coding region were prepared by PCR. For expression of the Ser78-phosphorylated MenT3 protein (MenT3_S78p), the *MenA3–MenT3* module was PCR amplified and cloned between the NdeI and XhoI sites of pET22b (Novagen), yielding pET22-MenA3T3. For expression of MenA3, the *MenA3* gene was also PCR amplified and cloned between the NdeI and XhoI sites of pET15sumo and the EcoRI and HindIII sites of pMAL-c6T (NEB, Japan), yielding the plasmids pET15sumo-MenA3 and pMAL-MenA3, respectively. pET15sumo was designed to express proteins fused with an N-terminal SUMO (small ubiquitin-related modifier) tag carrying the N-terminal hexahistidine (His_6) sequence (19). pMAL-MenA3 was designed to express the MenA3 protein with His_6-MBP at the N-terminal end.

The DNA fragment encoding MenT3 was cloned between the NdeI and HindIII sites of pBAD33.1 (ATCC87402), yielding pBAD33_MenT3. pBAD33_MenT3 variants with a mutation in the *MenT3* coding region were prepared by PCR.

Synthetic DNAs encoding *M. tuberculosis* $tRNA^{Ser}UGA$ and *E. coli* $tRNA^{Ala}GCC$ and its variants, downstream of the T7 RNA promoter, were purchased from Eurofins. Other plasmids for *in vitro* transcription of *M. tuberculosis* $tRNA^{Ser}$ variants were also purchased from Eurofins, and the DNA sequences of the genes used for *in vitro* transcription are listed in Supplementary Table S1. The oligonucleotide primers used for the PCR cloning and mutations are listed in Supplementary Table S2. *Escherichia coli* tRNA transcripts (20) were kind gift from Dr Shimizu at RIKEN, Japan.

Protein expression and purification

For expression of wild-type MenT3 (or catalytically inactive MenT3_D80A or other mutant MenT3 variants), *E. coli* BL21(DE3) (Novagen–Merck Millipore) was transformed with pET22-MenT3 (or pET22-MenT3_D80A or other mutant plasmids) and cultured until the OD_{660} reached ∼1.0. Protein expression was induced by the addition of 0.4 mM isopropyl-β-D-thiogalactopyranoside (IPTG), and the culture was continued for 3 h at 37°C. For expression of the Ser78-phosphorylated MenT3 protein (MenT3_S78p), *E. coli* BL21(DE3) was transformed with pET22-MenA3T3. Protein expression was induced by the addition of 0.1 mM of IPTG, and the culture was continued for 12 h at 20°C. For expression of SUMO-tagged or MBP (maltose-binding protein)-tagged MenA3, *E. coli* BL21(DE3) was transformed with pET15sumo-MenA3 or pMAL-MenA3, respectively, and protein expression was induced by the addition of 0.1 mM of IPTG, and the cultures were continued for 12 h at 20°C.

The harvested cells, expressing MenT3, MenT3_D80A and MenT3_S78p, were sonicated in Ni buffer [25 mM Tris–Cl, pH 7.0, 500 mM NaCl, 10% (v/v) glycerol, 20 mM imidazole, 5 mM β-mercaptoethanol] supplemented with 0.1 mM PMSF (phenylmethylsulfonyl fluoride) and 50 μg/ml lysozyme. The lysates were centrifuged at 30 000 × *g* and 4°C for 30 min, and the supernatants were applied to a Ni-NTA column (QIAGEN, Japan). The column was washed with Ni buffer, and the proteins were eluted with Ni buffer supplemented with 500 mM imidazole. The proteins were then applied to a HiTrap Heparin or HiTrap Q column (GE Healthcare, Japan). Finally, the proteins were purified on a HiLoad 16/60 Superdex 200 column (GE Healthcare, Japan), equilibrated with buffer containing 25 mM Tris–Cl (pH 7.0), 200 mM NaCl and 10 mM β-mercaptoethanol, and concentrated.

For the purification of MenA3 with a SUMO tag carrying His_6 at its N-terminus or MenA3 with an N-terminal MBP

tag and a C-terminal His_6 tag, the proteins were expressed and purified by Ni-NTA chromatography. Subsequently, the SUMO-tagged and MBP-tagged MenA3 proteins were purified as described above.

tRNA preparation

tRNA transcript variants were synthesized by T7 RNA polymerase, using plasmids linearized by MvaI digestion as templates. The tRNA transcripts were separated by polyacrylamide gel electrophoresis (PAGE) under denaturing conditions, excised from the gels and eluted from the gel slices using a Whatman® Elutrap (Whatman, Japan). Gel-purified tRNA transcripts were ethanol precipitated, rinsed with 70% (v/v) cold ethanol, dried and then stored at −30°C.

In vitro nucleotidyltransferase assay

The standard MenT3 nucleotidyltransferase activity assay was conducted at 37°C, in a reaction mixture containing 50 mM Tris–Cl (pH 8.5), 10 mM $MgCl_2$, 75 mM NaCl, tRNA transcript, 1 mM CTP [or [α-^{32}P]-CTP (PerkinElmer, Japan, 3000 Ci/mmol)] and MenT3 (or its variants). The specific conditions for each assay of nucleotidyltransfer to tRNA transcript variants by MenT3 (or its variants) are clearly described in either the text or figure legends. Reactions were quenched by the addition of an equal volume of formamide gel-loading buffer [95% (v/v) formamide, 0.02% (w/v) sodium dodecyl sulfate (SDS), 0.02% (w/v) bromophenol blue, 0.01% (w/v) xylene cyanol], and the tRNAs were separated by 10% (w/v) PAGE under denaturing conditions. For non-RI (Radio isotope) assays, the gels were stained with ethidium bromide, and tRNA band intensities were quantified by the Image Lab Software (Bio-Rad, version 3.0). For steady-state kinetic analyses, [α-^{32}P]-CTP or [α-^{32}P]-UTP (PerkinElmer, Japan) was used for the assays and the ^{32}P-labeled tRNA bands were quantified using a BAS-2000 or BAS-4000 imager (Fujifilm, Japan).

In vivo MenT3 toxicity assay

Escherichia coli strain MG1655 (NIG, Japan; ME7986) was transformed with pBAD33_MenT3 or its variants. The transformed cells were inoculated into LB medium containing 50 μg/ml chloramphenicol and 1% (w/v) glucose, and cultured at 37°C overnight. The toxicities of MenT3 and its variants were assessed using a spot assay. Overnight LB cultures were serially diluted, and 3-μl aliquots of the dilutions were spotted on LB agar plates containing 50 μg/ml chloramphenicol, supplemented with either 0.2% (w/v) arabinose or 1.0% (w/v) glucose. The plates were then incubated overnight at 37°C.

Preparation of aa-tRNAs and LC/MS spectrometry

Escherichia coli strain MG1655 was transformed with either pBAD33_MenT3 or the control plasmid pBAD33.1. The transformed cells were inoculated into LB medium supplemented with 50 μg/ml chloramphenicol and 1% (w/v) glucose, and cultured overnight at 37°C. The cultures were then diluted to an OD_{660} of 0.02 in LB (4 ml) supplemented with 50 μg/ml chloramphenicol, and further cultured at 37°C until the OD_{660} reached around 0.3. After 0.02% (w/v) arabinose was added, the cells were incubated for 10 min and then harvested. The cells were suspended in cold buffer, containing 50 mM NaOAc (pH 5.0), 0.5 mM EDTA and 0.2 M NaCl, and RNA was extracted using phenol saturated with 300 mM NaOAc (pH 5.2). RNAs were precipitated with isopropyl alcohol and then dissolved in 300 mM NaOAc (pH 5.2). aa-tRNAs were chemically acetylated using acetic anhydride (21–24), followed by ethanol precipitation. The RNA was dissolved in buffer containing 50 mM NaOAc (pH 5.0), 0.5 mM EDTA and 0.2 M NaCl. The RNA was loaded onto a Q-Sepharose Fast Flow column (GE Healthcare, Japan), and the resin was washed with buffer containing 50 mM NaOAc (pH 5.0), 0.5 mM EDTA and 0.3 M NaCl. The acetylated aa-tRNAs (Ac-aa-tRNAs) were eluted with buffer containing 50 mM NaOAc (pH 5.0), 0.5 mM EDTA and 0.6 M NaCl, precipitated with ethanol and rinsed with 70% (v/v) ethanol. The Ac-aa-tRNAs were digested with RNase One Ribonuclease (Promega, Japan) at 37°C for 60 min, in a reaction solution (25 μl) containing 25 mM NH_4OAc and 2.5 units of RNase One. The digests were subjected to liquid chromatography/mass spectrometry (LC/MS) analysis, as described previously (19,22,23,25).

Crystallization and structural determination of MenT3(D80A) in complex with CTP

To crystallize MenT3(D80A) in complex with CTP, 100 μM MenT3(D80A) was mixed with 10 mM CTP, and a 0.2-μl aliquot of the MenT3(D80A)–CTP mixture was mixed with 0.2 μl of reservoir solution, containing 0.2 M disodium malonate (pH 6.0) and 20% (w/v) PEG 3350. Crystals were obtained using the sitting-drop vapor diffusion method at 20°C.

The crystals were flash-cooled in a cryoprotectant solution consisting of 1.1× concentrated reservoir solution supplemented with 20% (v/v) ethylene glycol. Data sets were collected at beamline 17A at the Photon Factory at KEK, Japan, using the remote monitoring and diffraction evaluation system. The data were indexed, integrated and scaled with XDS (26). The crystal of MenT3(D80A)–CTP belongs to *P*1211, with three MenT3(D80A)–CTP complexes in the asymmetric unit cell. The initial phases were determined by the molecular replacement method, utilizing the structure of *apo* MenT3 [Protein Data Bank (PDB) ID: 6Y5U] (16) as the search model. The structures were refined with phenix.refine (27) and manually modified with Coot (28).

Finally, the structures were model-built and refined to an *R* factor of 18.8% (R_{free} = 24.1%) at a resolution of 2.1 Å for MenT3(D80A)–CTP. Detailed crystallographic data collection and refinement statistics are presented in Table 1.

Results

MenT3 incorporates CMP onto the 3′-CCA of tRNA

A previous report showed that MenT3 adds pyrimidine nucleotides (C or U) to the 3′-CCA of tRNAs (16). To assess the nucleotide specificity of MenT3, nucleotide incorporation was examined using the *M. tuberculosis* $tRNA^{Ser}$UGA (Mt $tRNA^{Ser}$) transcript as the substrate, with a high concentration of nucleotide (1 mM). The results indicated that CMP is efficiently incorporated into Mt $tRNA^{Ser}$, with several CMPs added to the 3′-end (Figure 1A). UMP is also incorporated, but only one UMP is added to the 3′-end of Mt $tRNA^{Ser}$, and the efficiency is much lower than CMP incorporation. Neither AMP nor GMP incorporation into Mt $tRNA^{Ser}$ was detected. The order of the nucleotide specificity of MenT3 is CTP ≫ UTP ⋙ ATP/GTP. The steady-state kinetics of

Table 1. Data collection and refinement statistics

	MenT3(D80A)–CTP
Data collection	
Space group	*P*1211
Cell dimensions	
a, *b*, *c* (Å)	59.96, 91.53, 85.06
α, β, γ (°)	90, 100.997, 90
Wavelength (Å)	1.0450
Resolution (Å)[a]	49.51–2.1 (2.175–2.1)
R_{sym}[a]	0.1376 (1.298)
I/σ_I[a]	13.11 (1.57)
$CC_{1/2}$[a]	0.998 (0.605)
Completeness (%)[a]	99.84 (99.18)
Redundancy[a]	7.0 (7.1)
Refinement	
Resolution (Å)	49.51–2.1
No. of reflections	52 643
R_{work}/R_{free} (%)	0.1878/0.2411
No. of atoms	
Protein	6618
Ligand	87
Water	356
B-factors (Å^2)	
Protein	35.68
Ligand	37.78
Water	39.36
Root-mean-square deviations	
Bond lengths (Å)	0.008
Bond angles (°)	1.10

[a]Values in parentheses are for the highest resolution shell.

nucleotide incorporation into Mt tRNA^{Ser} showed estimated K_m values for CTP and UTP of 136 ± 51.3 and 874.5 ± 291 μM, respectively, and estimated k_{cat} values for CTP and UTP of 0.058 ± 0.0072 and 0.022 ± 0.0038 s^{-1}, respectively (Figure 1B). The efficiency of UMP incorporation (k_{cat}/K_m) is ∼6% of that for CMP incorporation, with CTP proving to be a much better substrate than UTP for MenT3 *in vitro*. Thus, MenT3 exhibits highly specific CMP incorporation onto the 3′-CCA end of tRNAs and functions as a CTP-tRNA nucleotidyltransferase.

Structural basis of specific CTP recognition by MenT3

To elucidate the molecular basis of the nucleotide specificity of MenT3, we determined the crystal structure of the catalytically inactive mutant MenT3(D80A) in complex with CTP (Table 1). The expression of MenT3(D80A) in *E. coli* showed reduced toxicity compared to that of wild-type MenT3 (Supplementary Figure S1A and B). Therefore, to obtain a sufficient amount of the MenT3 protein for crystallization, we expressed and purified the mutant MenT3(D80A).

In the structure of MenT3(D80A) in complex with CTP, the electron density corresponding to CTP was clearly observed in the cleft between the N-terminal catalytic nucleotidyltransferase domain, containing antiparallel β-sheets with three possible catalytic carboxylates (D80, D82 and E146), and the C-terminal domain with five α-helices (Figure 1C). CTP extensively interacts with MenT3 in the cleft (Figure 1C).

Comparison of the catalytic core structure of MenT3(D80A) in complex with CTP and that of *Thermotoga maritima* CCA-adding enzyme (TmCCA) in complex with CTP (29) shows that the triphosphate group of CTP and the possible catalytic carboxylates (D80A, D82, and E146) in MenT3(D80A)–CTP superimposed well on the triphosphate group of CTP and the catalytic carboxylates (D55, D57, D99) in TmCCA–CTP, respectively (Supplementary Figure S1C). The position of the CTP relative to the carboxylates suggests that CTP in the present MenT3(D80A)–CTP structure binds within the incoming nucleotide site in the catalytic pocket (30) (Supplementary Figure S1C and D). The mutations of D82A and E146A in MenT3 also attenuated the toxicity of the mutant MenT3 when expressed in *E. coli* as the mutant D80A, compared with the toxicity of wild-type MenT3 (Supplementary Figure S1A). Thus, D80, D82 and E146 in MenT3 act as catalytic carboxylates.

The triphosphate of CTP hydrogen bonds with several amino acid residues. K79 and R205 hydrogen bond with the α-phosphate oxygen, K189 and H207 hydrogen bond with the β-phosphate oxygen, and R76 and H207 hydrogen bond with the γ-phosphate oxygen. The 2′-OH of the CTP ribose forms hydrogen bonds with E188, while the cytosine base stacks with the side chain of M122. The 4-NH_2 of the cytosine base forms a hydrogen bond with the main-chain carbonyl oxygen of P120, and the N_3 and O_2 atoms of the cytosine base hydrogen bond with the side chain of R238 (Figure 1D).

The CTP recognition by MenT3 in the present structure explains the nucleotide specificity of MenT3 for CTP (Figure 1A and B). In the model of UTP in the nucleotide-binding pocket of MenT3, the O_4 and N_3 atoms of the uracil base would not form hydrogen bonds with the main-chain carbonyl oxygens of P120 and R238, respectively, and only the O_2 atoms of uracil could form a hydrogen bond with R238 (Figure 1E). This explains the higher K_m value of UTP compared with that of CTP (Figure 1B). Consequently, UMP incorporation onto tRNA would not proceed efficiently (Figure 1A and B). The larger ATP and GTP could not bind to the pocket due to steric clashes with the residues composing the pocket (Figure 1E). Thus, neither ATP nor GTP could be substrates of MenT3 (Figure 1A).

A structural comparison between the *apo* MenT3 and CTP-bound forms of MenT3(D80A) revealed the structural differences in the loop between β3 and β4 (Figure 1F). In the CTP-bound MenT3(D80A), the loop shifts towards CTP by ∼7 Å as compared to the loop in the *apo* MenT3 structure, and the main-chain carbonyl oxygen of P120 in the loop forms a hydrogen bond with the 4-NH_2 of CTP (Figure 1F). In contrast, the conformations of R238, which hydrogen bonds with the N_3 and O_2 atoms of CTP bound to MenT3(D80A) (Figure 1F), are not significantly different between the *apo* MenT3 and CTP-bound forms of MenT3(D80A).

Mutations in CTP binding sites attenuate MenT3 activity

To examine the involvements of the CTP-interacting residues in the activity of MenT3, mutations were introduced into MenT3, and the toxicities of the mutants in *E. coli* were assessed upon expression. MenT3 was expressed under the control of the arabinose-inducible araBAD promoter (31). Wild-type MenT3 expression in *E. coli* is toxic and suppresses cell growth on agar plates and in liquid media (Supplementary Figure S1A and B).

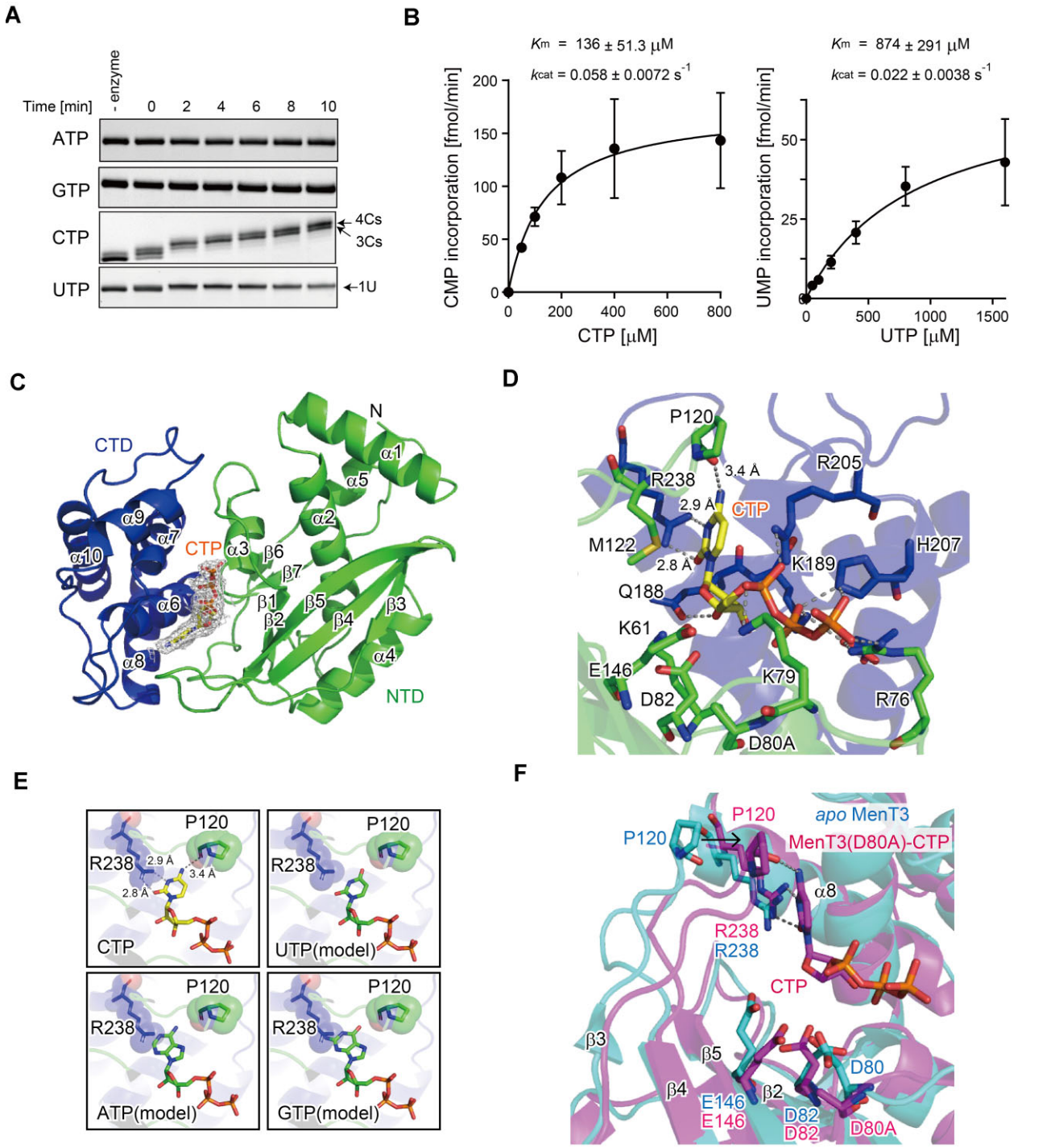

Figure 1. Incorporation of CMP onto tRNA and specific CTP recognition by MenT3. (**A**) CMP incorporation onto the 3′-CCA end of the *M. tuberculosis* $tRNA^{Ser}$ transcript. 0.5 μM $tRNA^{Ser}$ was incubated at 37°C with 0.01 μM MenT3 in the presence of 1 mM NTP (CTP, UTP, ATP or GTP), and the $tRNA^{Ser}$ was separated by 10% (w/v) PAGE under denaturing conditions. The gel was stained with ethidium bromide. (**B**) Steady-state kinetics of CMP (left) or UMP (right) incorporation into the *M. tuberculosis* $tRNA^{Ser}$ transcript by MenT3. The initial velocities of CMP (or UMP) incorporation into $tRNA^{Ser}$ (2.5 μM) by the enzymes (5 nM) were measured with various concentrations of [α-^{32}P]-CTP (0.1 Ci/mmol; 50–800 μM) or [α-^{32}P]-UTP (0.1 Ci/mmol; 50–1600 μM). (**C**) Overall structure of MenT3_D80A in complex with CTP. The N-terminal catalytic nucleotidyltransferase domain (NTD, residues 4–181) and the C-terminal domain (CTD, residues 182–291) are modeled. CTP resides in the cleft between the NTD and CTD and is depicted as stick model. The F_o–F_c omit map of CTP contoured at 3.0σ is shown (mesh). (**D**) A detailed view of CTP recognition by MenT3_D80A. NTD, CTD and CTP are colored as in panel (C). (**E**) Models of UTP, ATP and GTP binding in the nucleotide-binding pocket of MenT3. UTP, ATP and GTP are depicted as stick models. (**F**) Superimposition of the structure of the MenT3(D80A)–CTP (magenta) complex and *apo* MenT3 (cyan, PDB ID: 6Y5U). The arrow indicates the shift of the loop containing P120 between β3 and β4, upon CTP binding.

Consistent with the present structure, the mutations of residues interacting with CTP in MenT3 (Figure 1D) attenuated the toxicity of the mutant MenT3 when expressed in *E. coli*, compared with the toxicity of wild-type MenT3 (Figure 2A and B). The Ala mutation of R238, which forms hydrogen bonds with the N_3 and O_2 atoms of the CTP base (Figure 1D), especially weakened the toxicity of MenT3 (Figure 2A and B). The deletion of the loop between β3 and β4 (Δ117–125), which contains P120, and the mutation of M122 to Ala also attenuated the toxicity of MenT3 (Figure 2C and D).

The mutation of R238 to Ala and the deletion of the loop between β3 and β4 (Δ115–125) reduced the CMP incorporation into Mt tRNA^{Ser} *in vitro* (Figure 2E). The deletion of the loop containing P120 severely affected the CMP incorporation. The steady-state kinetics of CMP incorporation into Mt tRNA^{Ser} showed that the R238A mutation increased the K_m value of CTP for MenT3 to $\gg$1 mM (Figure 2F). Thus, the R238 residue in the catalytic pocket of MenT3 strengthens the affinity of MenT3 for CTP and dictates the specificity.

Altoghter, MenT3 functions as a CTP-tRNA nucleotidyltransferase toxin, and the CMP incorporation by MenT3 inactivates tRNAs and leads to the suppression of cell growth.

Phosphorylation of Ser78 in MenT3 by MenA3 reduces the MenT3 activity

The antitoxin MenA3 reportedly phosphorylates S78 of MenT3 and reduces the toxicity of MenT3 *in vivo* (14). Indeed, the MBP- or SUMO-tagged MenA3 protein phosphorylated wild-type MenT3, but not mutant MenT3(S78A) (Figure 3A). The purified MenT3 proteins expressed alone or co-expressed with MenA3 in *E. coli* were analyzed by Phos-tag gel SDS–PAGE, an electrophoresis technique capable of separating the phosphorylated and nonphosphorylated forms based on their phosphorylation levels (32). About 80% of the purified MenT3 protein co-expressed with MenA3 is phosphorylated, as judged from the band intensities of phosphorylated and nonphosphorylated MenT3 (Figure 3B). The complete separation and purification of phosphorylated and nonphosphorylated MenT3 proteins could not be achieved under the conditions employed in this study (see the 'Materials and methods' section).

Assays of CMP incorporation onto Mt tRNA^{Ser} by wild-type MenT3 and phosphorylated MenT3 (MenT3 co-expressed with MenA3; MenT3_S78p) showed that MenT3_S78p has reduced nucleotidyltransferase activity as compared to wild-type MenT3 (Figure 3C). The residual activity of MenT3_S78p would be due to the remaining ∼20% of unphosphorylated MenT3 (Figure 3B). The superimposition of the structure of MenT3(D80A)–CTP with that of MenT3_S78p (14,16) revealed that the negatively charged triphosphate of CTP, particularly the γ-phosphate, has electronic repulsion with the phosphorylated S78 of MenT3 (Figure 3D). The structure explains why the phosphorylation of S78 in MenT3 by MenA3 suppresses the MenT3 toxicity. CTP would not be able to bind to the active site of MenT3_S78p and attenuate its activity, leading to the reduced toxicity of MenT3 *in vivo*.

MenT3 expression diminishes the level of Ser-tRNA^{Ser} isoacceptors

Previous *in vitro* analyses showed that MenT3 incorporates pyrimidine nucleotides into transcripts of *M. tuberculosis* tRNA^{Ser} isoacceptors (Ser-1, -2, -3 and -4), tRNA^{Leu} (Leu-5) and *E. coli* tRNA^{Trp} (16). However, the tRNA substrates of MenT3 *in vivo* have not been analyzed, and thus the tRNA substrate preference and specificity of MenT3 have remained elusive.

We analyzed the changes in aa-tRNA levels *in vivo* upon the expression of MenT3 in *E. coli*. After induction of MenT3 expression in *E. coli*, aa-tRNAs were prepared under acidic conditions, and the α-NH_2 groups of the aminoacyl bonds were acetylated by acetic anhydride, converting them into stable Ac-aa-tRNAs (21). The Ac-aa-tRNAs were hydrolyzed with RNase One, and after the amounts of Ac-aa-A76 were quantified by LC/MS (19,22,23,25), the cellular level of each aa-tRNA was inferred from the amount of the corresponding Ac-aa-A76 fragment. Because MenT3 was unable to incorporate CMP onto the 3′-end of the *E. coli* tRNA^{Ala} transcript *in vitro*, as described below, the relative amounts of individual aa-tRNAs with or without induction of MenT3 expression were normalized against the relative amounts of Ala-tRNA^{Ala} with or without induction of MenT3 expression, respectively (Supplementary Figure S2). The results showed that, upon induction of MenT3 expression, the amounts of Ac-Ser-A76 (m/z = 397.15) were reduced to less than ∼10% of those detected under non-induced conditions (Figure 4A and B), while the amounts of other Ac-aa-A76s were unaffected (Supplementary Figure S2). These results are consistent with the previous *in vitro* observation that pyrimidine nucleotides are incorporated into the transcripts of *M. tuberculosis* tRNA^{Ser} isoacceptors preferentially (16). On the other hand, the amounts of Ac-Trp-A76 (m/z = 496.19), Ac-Tyr-A76 (m/z = 473.18) and Ac-Ile/Leu-A76 (m/z = 423.20) were not significantly reduced (Figure 4A and B).

Consistent with the *in vivo* analyses (Figure 4B), MenT3 preferentially and most efficiently incorporated CMP onto the *E. coli* tRNA^{Ser} transcript, among the 21 kinds of *E. coli* tRNA transcripts tested *in vitro* (Figure 4C). MenT3 slightly incorporated CMP onto *E. coli* tRNA^{Leu} and tRNA^{Tyr} transcripts, which both belong to the same class II tRNAs with longer variable loops as tRNA^{Ser}. However, the efficiencies of CMP incorporation onto these tRNAs *in vitro* were less than ∼5% of that onto the tRNA^{Ser} transcript. Thus, the specific and efficient addition of CMP to tRNA^{Ser} preferentially diminishes the level of Ser-tRNA^{Ser}s *in vivo* (Figure 4B).

The variable loop of tRNA^{Ser} is important for CMP incorporation by MenT3

The *in vivo* and *in vitro* analyses described above indicate that tRNA^{Ser} isoacceptors represent the primary target of MenT3 (Figure 4). To clarify the MenT3 recognition sites within tRNA^{Ser}, *M. tuberculosis* tRNA^{Ser}UGA (Mt tRNA^{Ser}) transcript variants were prepared (Figure 5A), and the incorporation of CMP into the Mt tRNA^{Ser} variants by MenT3 was examined *in vitro* (Figure 5B and C). In the variants, the acceptor stem, D-loop, anticodon stem, variable loop or TΨC stem of Mt tRNA^{Ser} was shortened or deleted (Figure 5A).

While shortening the anticodon stem (Δ-ANCS) slightly reduced the CMP incorporation, shortening the acceptor stem (Δ-ACCS) or the TΨC stem (Δ-TΨCS) drastically affected the CMP incorporation by MenT3 (Figure 5B). Steady-state kinetics of CMP incorporation into tRNA^{Ser} and its variants showed that the K_m values of MenT3 for Δ-ACCS and Δ-TΨCS were 1.70 ± 0.20 and 3.24 ± 0.41 μM, and the k_{cat}

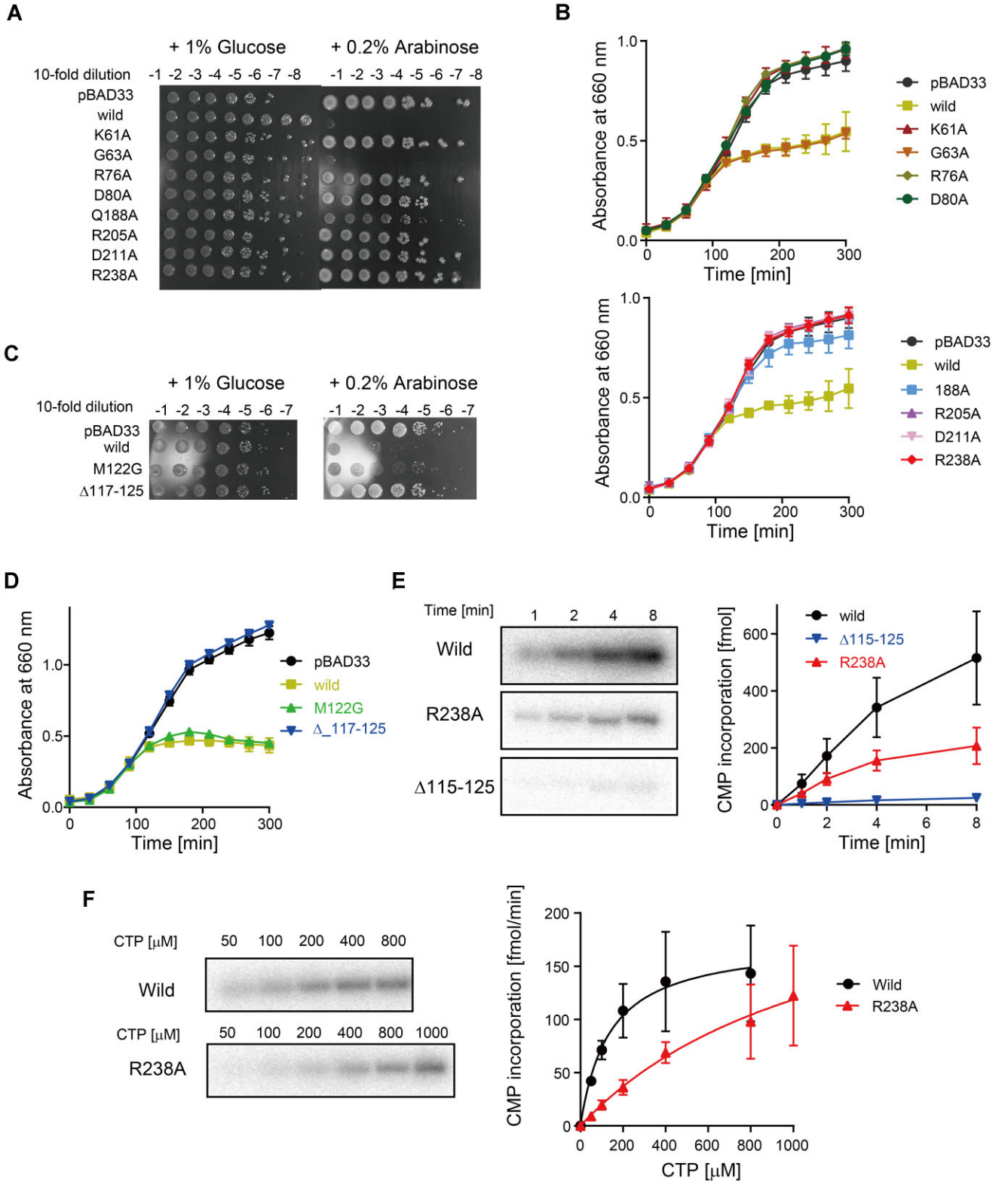

Figure 2. Reduction of MenT3 activity and toxicity by mutations in CTP binding pocket. (**A**) Attenuation of growth inhibition by mutant MenT3 expression in *E. coli*. Overnight cultures of *E. coli* MG1655 transformed with pBAD33 (control), pBAD33_MenT3 (wild) or its variants were serially diluted, and aliquots were spotted on LB agar plates containing 50 μg/ml chloramphenicol and supplemented with 1% (w/v) glucose (left panel) or 0.2% (w/v) arabinose (right panel). (**B**) Growth curves of *E. coli* MG1655 transformed with pBAD33 (control), pBAD33_MenT3 (wild) or its variants in panel (A). Arabinose was added (final concentration 0.1%) to the medium, and the culture was continued at 37°C. (**C**) Attenuation of growth inhibition by mutant MenT3 expression in *E. coli*, measured as in panel (A). (**D**) Growth curves of *E. coli* MG1655 transformed with pBAD33 (control), pBAD33_MenT3 (wild) or its variants in panel (C). (**E**) CMP incorporation into the *M. tuberculosis* $tRNA^{Ser}$ transcript (2.5 μM) by wild-type MenT3 and its variants (5 nM) at 100 μM [α-^{32}P]-CTP. (**F**) Steady-state kinetics of CMP incorporation into the *M. tuberculosis* $tRNA^{Ser}$ transcript by wild-type MenT3 and R238A mutant. The initial velocities of CMP incorporation into $tRNA^{Ser}$ (2.5 μM) by the enzymes (5 nM) were measured with various concentrations of [α-^{32}P]-CTP (0.1 Ci/mmol; 50–1000 μM). Error bars in the graphs in panels (B), (D), (E) and (F) represent SDs of more than three independent experiments, and the data are presented as mean values ± standard deviation (SD).

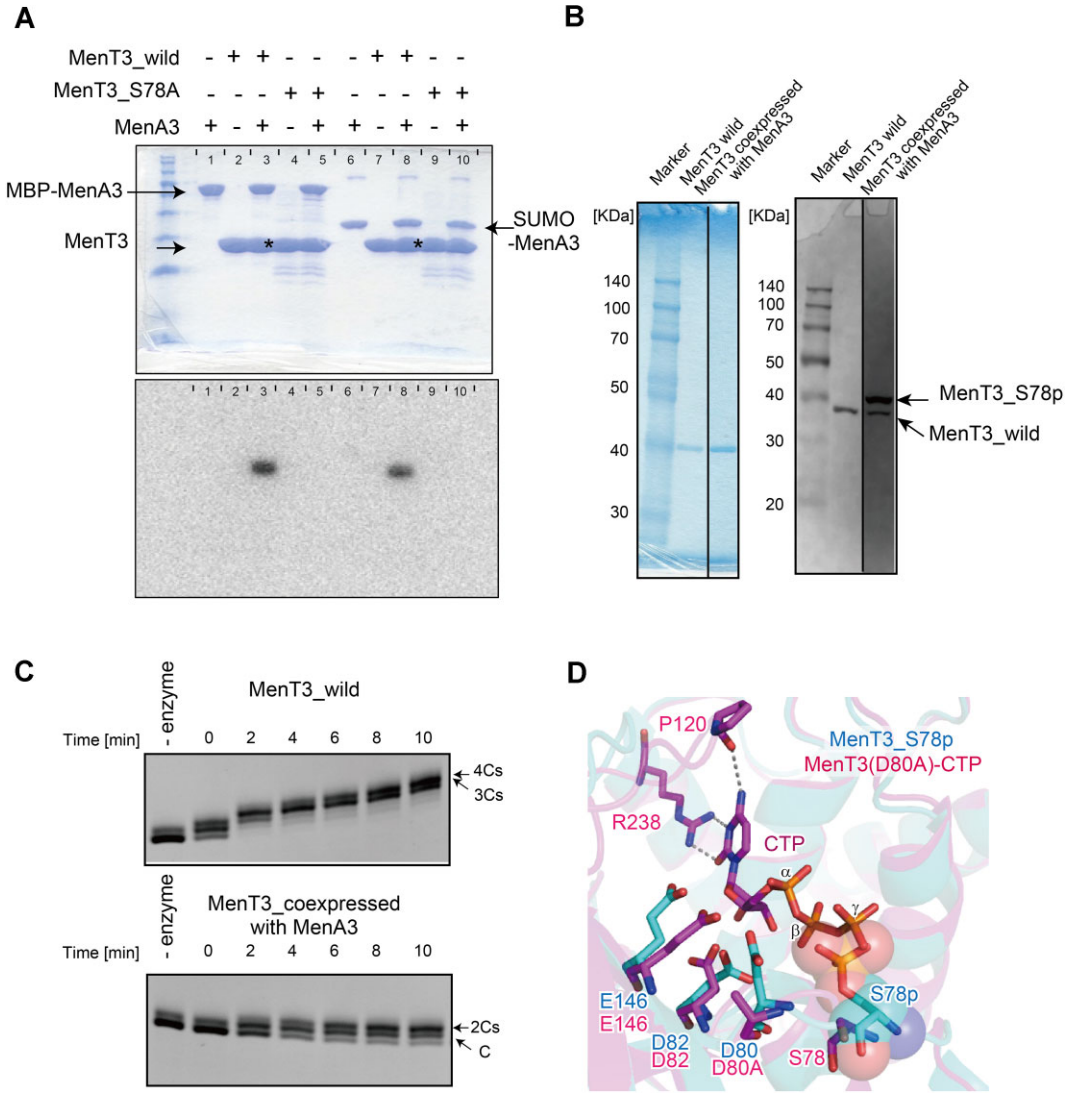

Figure 3. MenA3 phosphorylates MenT3 and reduces its activity. (**A**) Phosphorylation of Ser78 of MenT3 by MenA3 *in vitro*. Wild-type MenT3 or MenT3_S78A (20 μM) was incubated with 5 μM MBP-tagged (lanes 1, 3 and 5) or SUMO-tagged (lanes 6, 8 and 10) MenA3 in the presence of 1 mM [γ-^{32}P] ATP, at 37°C for 3 h. Reaction solutions were separated by 10% (w/v) SDS–PAGE and stained with Coomassie Brilliant Blue (CBB) (upper panel). ^{32}P-labeled protein bands were detected by a BASS-2000 imager (Fujifilm, Japan) (lower panel). Asterisks in the gel (upper panel) indicate the ^{32}P-labeled protein bands (MenT3_wild). (**B**) Separation of purified MenT3_wild and Ser78-phosphorylated MenT3 (MenT3_S78p) by 12.5% (w/v) Super-Sep gel (Wako, Japan; left gel) and by 12.5% (w/v) Phos-tag gel (Wako, Japan; right gel), stained with CBB. About 80% of MenT3 is phosphorylated when co-expressed with MenA3 in *E. coli*, as judged from the band intensities of phosphorylated and nonphosphorylated MenT3 in the Phos-tag gel. (**C**) Phosphorylation of MenT3 reduces its activity. The *M. tuberculosis* tRNA^{Ser} transcript (0.5 μM) was incubated with 0.01 μM MenT3_wild (upper panel) or MenT3_S78p (lower panel) in the presence of 1 mM CTP at 37°C, and separated by 10% (v/w) PAGE under denaturing conditions. The residual activity of MenT3 co-expressed with MenA3 is due to the unphosphorylated MenT3 in the preparation, as shown in the right gel of panel (B). (**D**) Superimposition of the structure of MenT3(D80A)–CTP (magenta) with that of MenT3 with phosphorylated Ser78 (MenT3_S78p, cyan, PDB ID: 6Y5U) (16). The phosphorylated Ser78, shown in a sphere model, clashes with the triphosphate of CTP (stick model, magenta).

values were 0.135 ± 0.008 and 0.130 ± 0.01 s^{-1}, respectively. Thus, the reduction of CMP incorporation into Δ-ACCS or Δ-TΨCS by MenT3 is mainly due to the decreased k_{cat} (the K_m value for wild-type Mt tRNA^{Ser} was 1.01 ± 0.13 μM and the k_{cat} value was 0.959 ± 0.055 s^{-1}) (Figure 5C). The shortening of the variable loop (Δ-VL) also reduced the CMP incorporation by MenT3 (Figure 5B), and the K_m value for Δ-VL was 0.75 ± 0.10 μM and the k_{cat} value was 0.234 ± 0.012 s^{-1}. Thus, the reduced CMP incorporation into Δ-VL also resulted from the decreased k_{cat}, as in Δ-ACCS and Δ-TΨCS (Figure 5C). Shortening the D-loop (Δ-DL) moderately reduced the CMP incorporation by MenT3 (Figure 5B), with the K_m and k_{cat} values being 0.835 ± 0.048 μM and 0.431 ± 0.010 s^{-1}, respectively. Accordingly, the reduced CMP incorporation is also due to the decreased k_{cat} (Figure 5C).

These results collectively imply that the tRNA core structure–ternary interaction between the D-loop and TΨC loop, the proper length of the acceptor–TΨC stem-loop and the longer variable loop of Mt tRNA^{Ser} are required for efficient CMP incorporation onto the 3′-end of tRNA^{Ser}. In particular, the longer variable loop of Mt tRNA^{Ser} contributes to the catalysis, probably through the proper positioning of tRNA^{Ser} on the surface of MenT3 for efficient CMP incorporation, as discussed below. Consistent with the importance of the long variable loop of Mt tRNA^{Ser} for efficient CMP incorporation by MenT3, while MenT3 does not incorporate

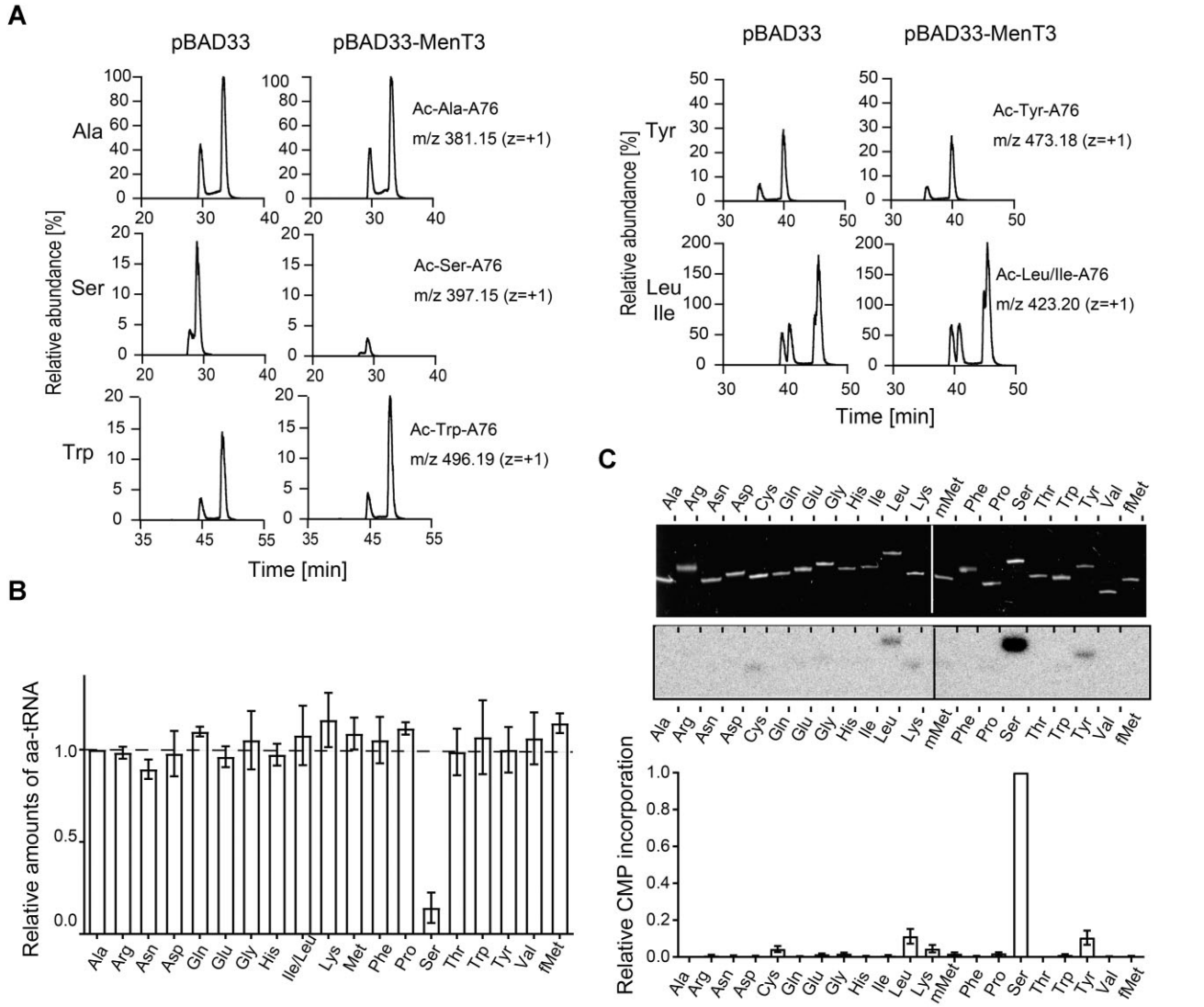

Figure 4. Reduction of Ser-tRNA^{Ser} levels upon MenT3 induction *in vivo*. (**A**) LC/MS analysis of RNase One-digested fragments of Ac-aa-tRNAs prepared from aa-tRNAs from *E. coli* with (pBAD33_MenT3) or without (pBAD33, control) induction of MenT3. The amount of each Ac-aa-A76 derived from aa-tRNA prepared from cells with or without MenT3 induction is expressed relative to Ac-Ala-A76 in cells with or without induction of MenT3, respectively. (**B**) Change of relative amounts of each aa-tRNA in *E. coli* after MenT3 induction. The relative amount of each aa-tRNA in *E. coli* with MenT3 induction was normalized against the amount of the corresponding aa-tRNA in *E. coli* without induction. (**C**) [α-^{32}P]-CMP incorporation in 21 kinds of *E. coli* tRNA transcripts (upper panel) (20) by MenT3 *in vitro*. Each tRNA transcript (0.5 μM) was incubated with 5 nM MenT3 and 1 mM [α-^{32}P]-CTP (0.1 Ci/mmol) at 37°C for 4 min. ^{32}P-labeled tRNAs were separated by denaturing PAGE, and the ^{32}P-labeled tRNA (middle panel) bands were quantified using a BAS-2000 imager (lower graph). Error bars in the graphs in panels (B) and (C) represent SDs of more than three independent experiments, and the data are presented as mean values ± SD.

any CMPs onto the *E. coli* tRNA^{Ala} transcript *in vitro* (Figures 4C and 5D), a mutant chimeric tRNA^{Ala} transcript, the Ec tRNA^{Ala}_chimera (Figure 5A) carrying the variable loop of Mt tRNA^{Ser}, incorporates CMP (Figure 5D). The efficiency of CMP incorporation into the Ec tRNA^{Ala}_chimera is ∼45% of that into Mt tRNA^{Ser} (Figure 5C). The K_m value of MenT3 for the Ec tRNA^{Ala}_chimera was 0.212 ± 0.023 μM, and the k_{cat} value was 0.086 ± 0.005 s^{-1}. These results collectively highlight the importance of the longer variable loop of Mt tRNA^{Ser} for efficient CMP incorporation by MenT3.

tRNA docking model onto MenT3

The surface electrostatic potential of MenT3 showed that positively charged residues form clusters on the same surface where the CTP resides, particularly in the nucleotidyltransferase domain (Figure 6A). To investigate the involvement of these positively charged residues in the MenT3 activity, mutations were introduced into MenT3, and the toxicities of the mutants in *E. coli* were assessed upon expression. Notably, the R13A, R16A, R128A and K132A mutations attenuated the MenT3 toxicity when expressed in *E. coli* (Figure 6B and C). Furthermore, the R13AR16A and R128AK132A mutations of MenT3 reduced CMP incorporation into Mt tRNA^{Ser} *in vitro* (Figure 6D). The initial velocities of CMP incorporation by the MenT3 mutants proceeded linearly up to 3 μM of Mt tRNA^{Ser}, and thus the mutations (R13AR16A and R128AK132A) increased the K_m value (≫3 μM) of MenT3 for Mt tRNA^{Ser} and decreased the k_{cat} value as well (Figure 6D). The R32AR35A mutation reduced the MenT3 activity. The K_m value of the mutant MenT3_ R32AR35A for Mt tRNA^{Ser} was 1.18 ± 0.38 μM and the k_{cat} value was

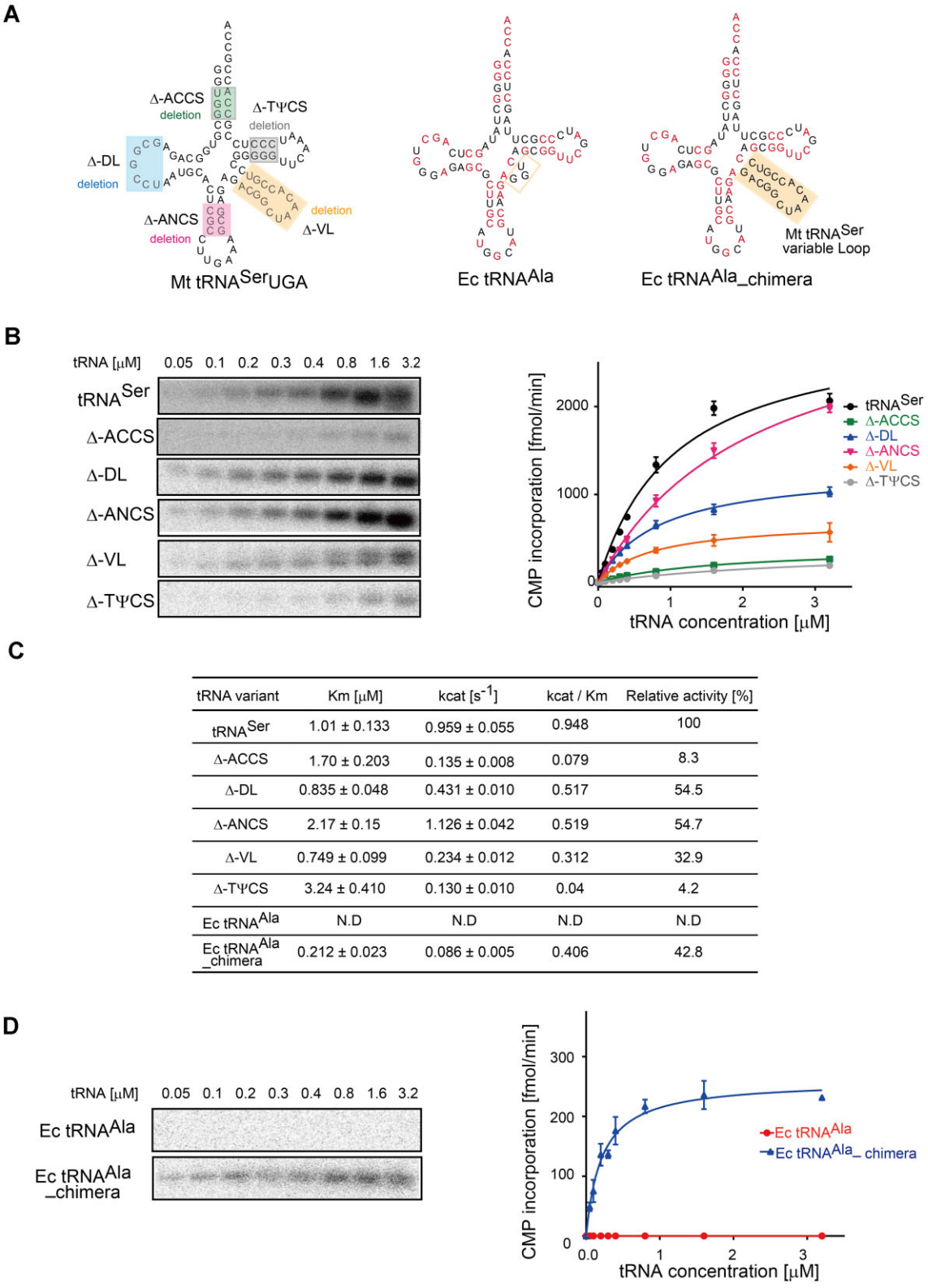

tRNA variant	Km [μM]	kcat [s^{-1}]	kcat / Km	Relative activity [%]
$tRNA^{Ser}$	1.01 ± 0.133	0.959 ± 0.055	0.948	100
Δ-ACCS	1.70 ± 0.203	0.135 ± 0.008	0.079	8.3
Δ-DL	0.835 ± 0.048	0.431 ± 0.010	0.517	54.5
Δ-ANCS	2.17 ± 0.15	1.126 ± 0.042	0.519	54.7
Δ-VL	0.749 ± 0.099	0.234 ± 0.012	0.312	32.9
Δ-TΨCS	3.24 ± 0.410	0.130 ± 0.010	0.04	4.2
Ec $tRNA^{Ala}$	N.D	N.D	N.D	N.D
Ec $tRNA^{Ala}$ _chimera	0.212 ± 0.023	0.086 ± 0.005	0.406	42.8

Figure 5. The variable loop of $tRNA^{Ser}$ is crucial for CMP incorporation by MenT3. (**A**) Nucleotide sequences of *M. tuberculosis* $tRNA^{Ser}$UGA (Mt $tRNA^{Ser}$UGA) and its variants. The nucleotides deleted from the acceptor stem (Δ-ACCS), anticodon stem (Δ-ANCS), D-loop (Δ-DL), TΨC stem (Δ-TΨCS) or variable loop (Δ-VL) are highlighted (left panel). Nucleotide sequences of *E. coli* $tRNA^{Ala}$ (Ec $tRNA^{Ala}$) and its variant with the variable loop of Mt $tRNA^{Ser}$ (Ec $tRNA^{Ala}$_chimera). The common nucleotides between *E. coli* $tRNA^{Ala}$ and Mt $tRNA^{Ser}$ are shown in red. (**B**) Steady-state kinetics of CMP incorporation onto the 3′-CCA end of the Mt $tRNA^{Ser}$ transcript and its variants in panel (A). Reaction mixtures containing various concentrations of Mt $tRNA^{Ser}$ and its variants (0.05–3.2 μM) were mixed with 5 nM MenT3 and 1 mM [α-^{32}P]-CTP (0.1 Ci/mmol) and incubated at 37°C for 4 min. (**C**) Summary of kinetic parameters. N.D., not determined. (**D**) The steady-state kinetics of CMP incorporation onto the 3′-CCA end of Ec $tRNA^{Ala}$ transcript and Ec $tRNA^{Ala}$_chimera, determined as in panel (B). Error bars in the graphs in panels (B) and (D) represent SDs of more than three independent experiments, and the data are presented as mean values ± SD.

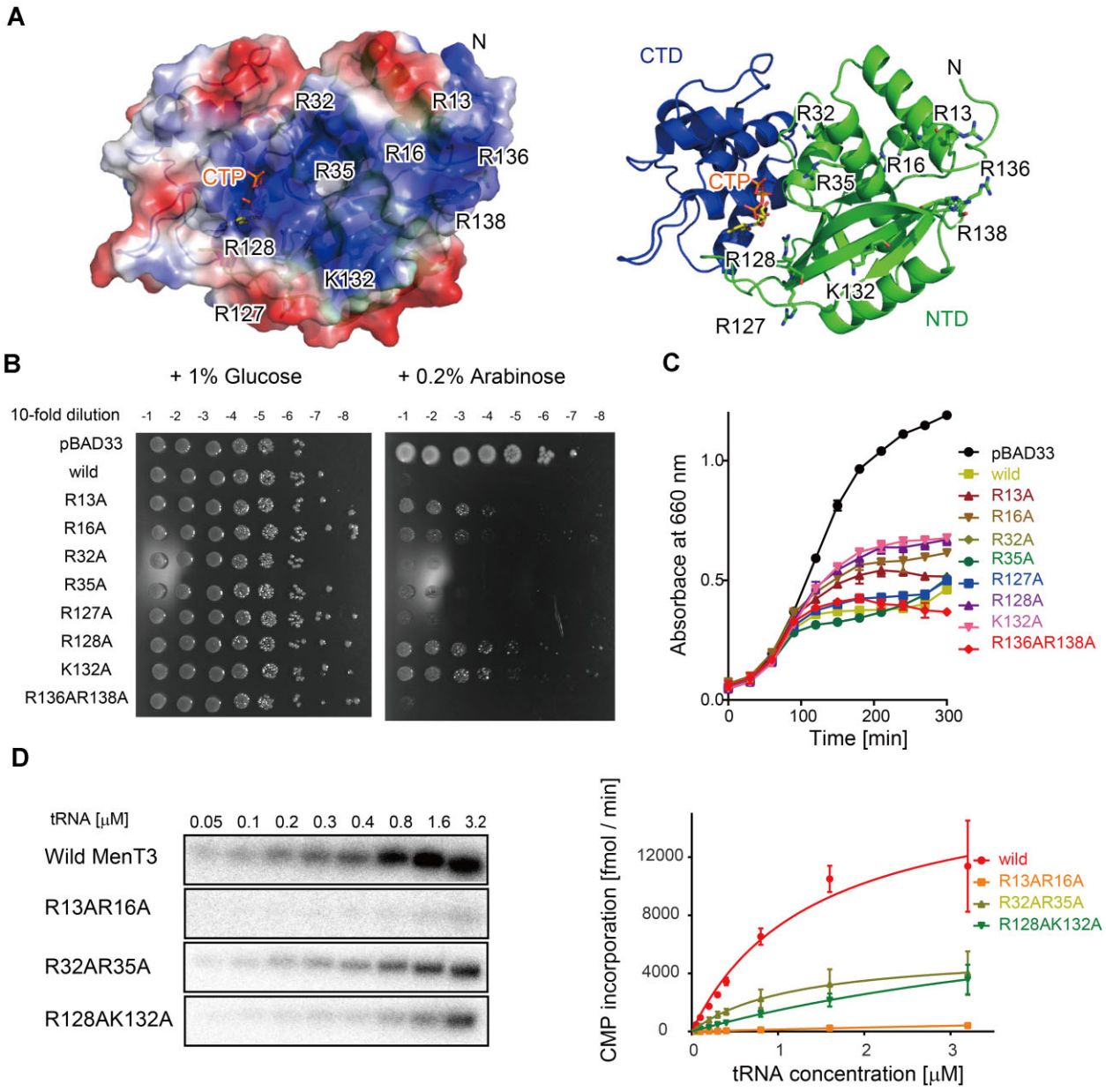

Figure 6. tRNA binding region in MenT3. (**A**) The surface electrostatic potential of MenT3. The positively and negatively charged areas are colored blue and red, respectively. The positive resides are clustered in the nucleotidyltransferase domain and on the same side where CTP binds. (**B**) Attenuation of growth inhibition by mutant MenT3 expression. Overnight cultures of *E. coli* MG1655 transformed with pBAD33_MenT3 (wild) or its variants were serially diluted, and the dilutions were spotted on LB agar plates, as in Figure 2A. (**C**) Growth curves of *E. coli* MG1655 transformed with pBAD33_MenT3 (wild) or its variants in panel (B), as in Figure 2B. (**D**) Steady-state kinetics of CMP incorporation into the *M. tuberculosis* $tRNA^{Ser}$ transcript by wild-type MenT3 and MenT3 variants. The initial velocities of CMP incorporation into $tRNA^{Ser}$ by wild-type MenT3 and its variants (5 nM) were measured with 1 mM [α-^{32}P]-CTP (0.1 Ci/mmol) and various concentrations of $tRNA^{Ser}$ transcript (0.05–3.2 μM) for 4 min. Error bars in the graphs in panels (C) and (D) represent SDs of more than three independent experiments, and the data are presented as mean values ± SD.

0.462 ± 0.086 s^{-1}. The K_m value of the wild-type MenT3 for Mt $tRNA^{Ser}$ was 1.45 ± 0.16 μM and the k_{cat} value was 1.40 ± 0.32 s^{-1}. Thus, the mutation decreases the k_{cat} value.

A tRNA docking model onto the positively charged area of MenT3 was built. A tRNA with a longer variable loop, human $tRNA^{Sec}$ (33) (PDB ID: 3A3A), was manually modeled, with the 3′ portion of the tRNA proximal to the active site where CTP binds (Figure 7A). In the model, the acceptor–TΨC stem of the tRNA, the top half of the tRNA molecule, interacts with the positively charged region, while the longer variable loop of tRNA is in the proximity of the N-terminal positively charged region. The N-terminal region of MenT3 would interact with the variable loop of $tRNA^{Ser}$ during CMP incorporation onto the 3′-CCA of $tRNA^{Ser}$. Consistently, the deletion of the N-terminal positively charged region (residues 2–11: ΔN_2–11) attenuated the toxicity of MenT3 when expressed in *E. coli* (Figure 7B and C). Furthermore, the deletion of the N-terminal positively charged region (Δ_2–11) abolished the CMP incorporation into Mt $tRNA^{Ser}$ *in vitro* (Figure 7D). The interaction between the variable loop of Mt $tRNA^{Ser}$ and the N-terminal region of MenT3 would prevent the tRNA molecule from dis-

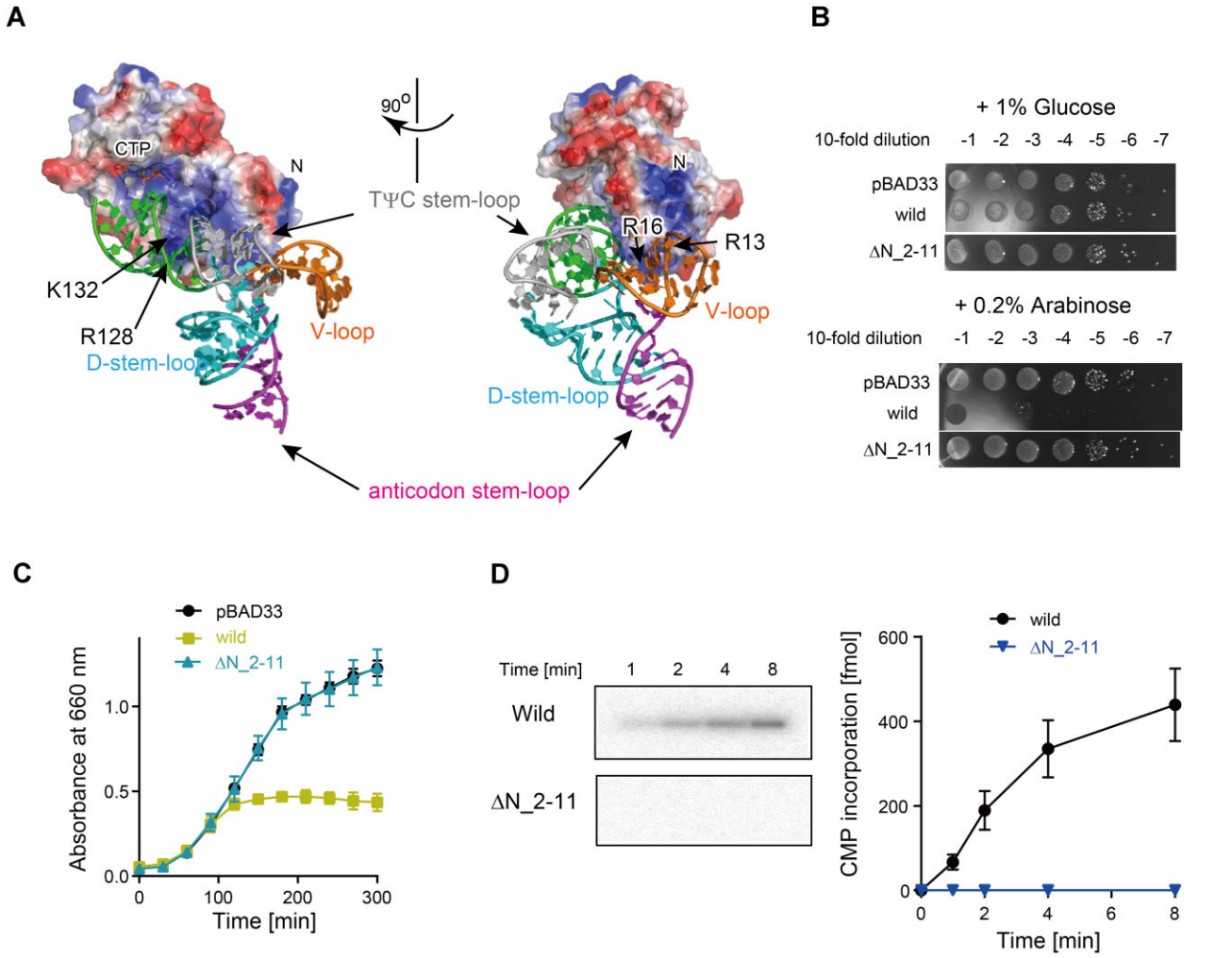

Figure 7. A model of tRNA binding to MenT3. (**A**) tRNA docking model. Human $tRNA^{Sec}$ (33) (PDB ID: 3A3A) was manually modeled onto MenT3. The acceptor stem-loop, D-stem-loop, anticodon stem-loop, variable loop and TΨC stem-loop are colored green, cyan, magenta, orange and gray, respectively. The 3′-ends are not fully modeled in the structure. (**B**) Attenuation of growth inhibition by the N-terminal deletion mutant MenT3 (Δ_2–11) expression, as in Figure 2A. (**C**) Growth curves of *E. coli* MG1655 transformed with pBAD33_MenT3 (wild) or its variants in panel (B). (**D**) CMP incorporation into the *M. tuberculosis* $tRNA^{Ser}$ transcript (1.0 μM) by wild-type MenT3 and MenT3_Δ_2–11 (5 nM) at 1 mM [α-^{32}P]-CTP. Error bars in the graph in panels (C) and (D) represent SDs of more than three independent experiments, and the data are presented as mean values ± SD.

lodging from the surface of MenT3, thus modulating the relocation of the 3′-CCA of tRNA within the active site of MenT3 and facilitating efficient CMP incorporation.

Discussion

MenT3, recently identified in human pathogen *M. tuberculosis*, reportedly incorporates pyrimidines (CMP/UMP) at the 3′-end of tRNAs, blocks the aminoacylation of tRNAs and inhibits protein synthesis (16). In this study, to clarify the molecular mechanism of its substrate specificity in detail, we analyzed the structure and function of MenT3.

MenT3 specifically incorporates CMPs (Figure 1A and B), and the structure of MenT3 in complex with CTP revealed the specific nucleotide-binding pocket suitable for the accommodation of CTP (Figure 1D). The 4-NH_2 and the O_2 and N_3 atoms of CTP form hydrogen bonds with the main-chain carbonyl oxygen of P120 and the side chain of R238, respectively. The CTP recognition mechanism by MenT3 is different from that of the class II CCA-adding enzyme, where the 4-NH_2 and the N_3 atom form hydrogen bonds with the Asp and Arg in the catalytic pocket, respectively (29,34–36). Extensive attempts to obtain the crystal of MenT3 in complex with UTP were unsuccessful, even under the conditions in which MenT3–CTP crystals were obtained, implying the weaker interaction between UTP and MenT3. ATP and GTP are too large and cannot be accommodated in the pocket (Figure 1E). Although UTP might bind to the catalytic pocket in the presence of UTP alone (Figure 1E), in the presence of all four nucleotides CMP would be predominantly incorporated onto the 3′-end of tRNAs. Thus, MenT3 specifically incorporates CMP onto the 3′-end of tRNAs, using the CTP-specific nucleotide-binding pocket and MenT3 is a CTP-specific nucleotidyltransferase toxin.

The change in the aa-tRNA levels upon MenT3 expression in *E. coli* showed that the level of Ser-$tRNA^{Ser}$ isoacceptors specifically decreased to <10% of that without MenT3 induction (Figure 4A and B). This reduction of Ser-$tRNA^{Ser}$ isoacceptor levels *in vivo* is quite distinct, and other aa-tRNA levels are not affected (Figure 4B). Consistent with the *in vivo* observations, the *in vitro* CMP incorporation onto 21 kinds of *E. coli* tRNA transcripts demonstrated that CMPs are most

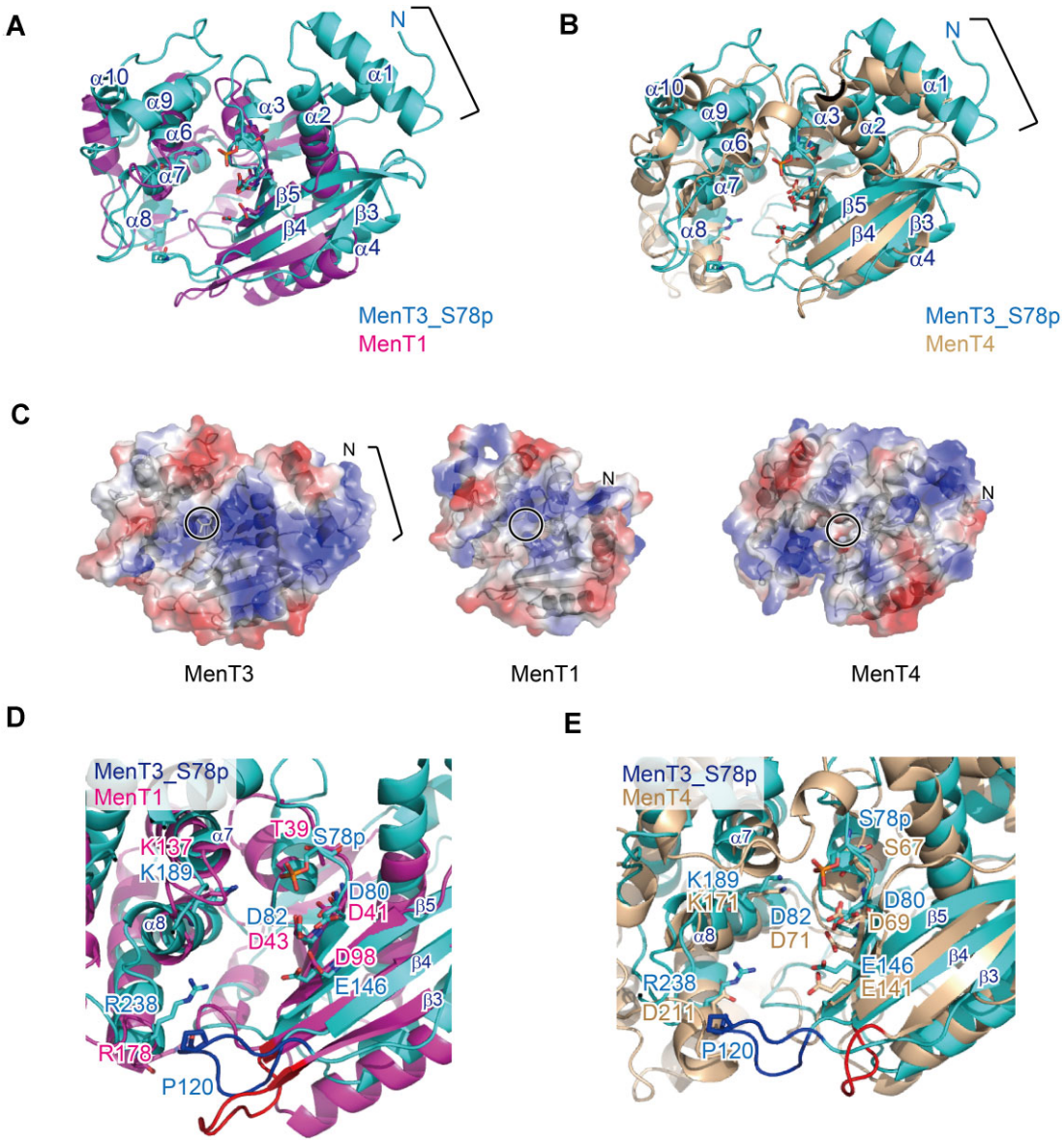

Figure 8. Structural comparisons between MenT3 and MenT1/MenT4. Superimposition of the overall structures of (**A**) MenT1 (magenta, PDB ID: 8AN4) (17) and MenT3_S78p (cyan, PDB ID: 6Y5U) (16) and (**B**) MenT3 (cyan) and MenT4 (wheat, PDB ID: 5Y56) (17). (**C**) The surface electrostatic potentials of MenT toxins. The active sites are circled. Positively and negatively charged areas are colored blue and red, respectively. (**D**) Superimposition of the catalytic pocket structures of MenT1 (magenta) and MenT3_S78p (cyan). The loop (residues 117–125) between β3 and β4 in MenT3 is colored blue, and the corresponding loop (residues 72–81) in MenT1 is colored red. (**E**) Superimposition of the catalytic pocket structures of MenT3_S78p (cyan) and MenT4 (wheat). The loop (residues 117–125) between β3 and β4 in MenT3 is colored blue, and the corresponding loop (residues 102–107) in MenT4 is colored red.

efficiently incorporated into $tRNA^{Ser}$ (Figure 4C). This is consistent with the previous data showing that MenT3 incorporates CMPs onto *M. tuberculosis* $tRNA^{Ser}$ transcript preferentially (16). Thus, CMP incorporation onto the 3′-CCA end of $tRNA^{Ser}$ reduces the level of Ser-$tRNA^{Ser}$ upon MenT3 expression. Collectively, MenT3 is a CTP:tRNA nucleotidyltransferase toxin specifically targeting $tRNA^{Ser}$ isoacceptors. We also showed that the phosphorylation of MenT3 by MenA3 indeed reduces the CMP incorporation onto the 3′-end of tRNA *in vitro* (Figure 3C) and provided the molecular basis for the lower activity of the phosphorylated MenT3_S78p (Figure 3D) and its lower toxicity (14).

The structures and sequences of the longer variable loop in $tRNA^{Ser}$ isoacceptors are crucial for efficient CMP addition to $tRNA^{Ser}$ isoacceptors by MenT3 (Figure 5). The tRNA docking model onto MenT3 (Figure 7A) suggests that the longer variable loop would interact with the N-terminal positively charged area of the nucleotidyltransferase domain. Therefore, the $tRNA^{Ser}$ acceptor–TΨC stem stably binds to the MenT3 surface, and the 3′-CCA of $tRNA^{Ser}$ would be properly positioned in the active site for efficient CMP incorporation. Consistently, the deletion of the N-terminal positively charged region (Δ_2–11) attenuated the toxicity of MenT3 when expressed in *E. coli* (Figure 7B and C) and abolished the CMP incorporation into Mt $tRNA^{Ser}$ *in vitro* (Figure 7D). Upon tRNA binding, the N-terminal region would relocate to interact with the variable region of $tRNA^{Ser}$.

Other tRNAs without the longer variable loop might bind to MenT3, but the 3′-CCA of tRNAs would not be appropriately located within the active site for CMP incorporation,

and thereby CMPs are not incorporated. The longer variable loop of $tRNA^{Ser}$ would also serve as an anchor that prevents its displacement from the surface of MenT3 for efficient CMP incorporation. Thus, the longer variable loop of $tRNA^{Ser}$ moderates the processibility as well as the catalysis of CMP incorporation onto the 3′-end of $tRNA^{Ser}$ by MenT3.

Bacterial $tRNA^{Ser}$ belongs to the class II tRNAs, including $tRNA^{Ser}$, $tRNA^{Leu}$, $tRNA^{Tyr}$ and $tRNA^{Sec}$ in bacteria, which all have longer variable loops than other tRNA species. *In vitro*, CMPs were slightly incorporated into *E. coli* $tRNA^{Tyr}$ and $tRNA^{Leu}$ transcripts, although the efficiencies were less than ∼5% of the CMP incorporation into $tRNA^{Ser}$ (Figure 4C). However, *in vivo*, the levels of Leu-$tRNA^{Leu}$ and Tyr-$tRNA^{Tyr}$ were not reduced when MenT3 was expressed in *E. coli* (Figure 4A and B). Thus, not only the presence of the longer variable loop but also the sequence and/or structure of the loops and/or other parts of the sequence in $tRNA^{Ser}$ would together dictate the specificity of MenT3 for tRNA substrates.

Quite recently, it was reported that MenT1 can incorporate CMP onto the 3′-CCA of tRNAs from *M. tuberculosis*, *E. coli* and *M. smegmatis in vitro* (17). Deep sequencing of the MenT1 and MenT4 reaction products using an *M. smegmatis* tRNA mixture as substrates showed that MenT1 and MenT4 specifically incorporate CMPs and GMPs, respectively, onto the 3′-CCA end of tRNA without preferences (17). Thus, the substrate specificities of MenT tRNA nucleotidyltransferase toxins for nucleotides and tRNA species are diverse among MenT1, MenT3 and MenT4.

The overall structural comparison between MenT3 and MenT1/MenT4 highlights the extended N-terminal positively charged region of MenT3 (Figure 8A and B) and the different surface charge distributions between MenT3 and MenT1/MenT4 (Figure 8C). As described above, the longer variable loop of $tRNA^{Ser}$ could interact with the N-terminal positively charged region of MenT3, and this interaction would be crucial for the specific recognition of $tRNA^{Ser}$ and the efficient CMP incorporation (Figures 5B–D and 7B–D). Thus, the distinct specificities toward tRNA substrates between MenT3 and MenT1/MenT4 might be partly governed by the different N-terminal structures, and MenT1 and MenT4 can bind to any tRNA species without preferences and with broad tRNA specificities.

The superimposition of the catalytic core structures of MenT1 and MenT3 suggests that, like MenT3, MenT1 could specifically recognize CTP. R238, which recognizes the O_2 and N_3 atoms of CTP in MenT3, corresponds to R178 in MenT1 (Figure 8D). The main-chain carbonyl oxygen of P120, in the loop between β3 and β4 of MenT3, interacts with the 4-NH_2 of CTP. The corresponding loop in MenT1 has almost the same length (Figure 8D). Thus, MenT1 would use the same mechanism for the specific recognition of CTP as MenT3. In contrast, the superimposition of the catalytic core structures of MenT3 and MenT4 suggests that the loop of MenT4 corresponding to the loop between β3 and β4 of MenT3 is shorter (Figure 8E), and that the residue corresponding to R238, which recognizes the O_2 and N_3 atoms of CTP in MenT3, is not present in MenT4. Instead, Asp211 is positioned at that position in MenT4 (Figure 8E). Thus, MenT4 has a different nucleotide specificity from MenT3. The mechanism of GTP recognition by MenT4 remains elusive and awaits further structural analysis of its complex with GTP.

In summary, we have elucidated the molecular basis for the nucleotide specificity of MenT3 for CTP and demonstrated that $tRNA^{Ser}$ acceptors are its primary target. The longer variable loop structures and/or the sequences of $tRNA^{Ser}$ isoacceptors play a crucial role in determining the tRNA substrate specificity of MenT3 and the N-terminal region of MenT3 would interact with the variable loop of $tRNA^{Ser}$ isoacceptors. The exact mechanism of substrate $tRNA^{Ser}$ recognition by MenT3, as well as substrate recognition by MenT1 and MenT4, remains to be fully clarified and awaits further structural analyses of these MenT toxins in complex with nucleotide and/or tRNA substrates.

Data availability

Coordinate and structure factor for the crystal structure of MenT3(D80A)–CTP have been deposited in the PDB, under the accession number 8XHR.

Supplementary data

Supplementary Data are available at NAR Online.

Acknowledgements

We thank the beamline staff of BL-17A (KEK, Tsukuba) for technical assistance during data collection. We thank Yoshihiro Shimizu (RIKEN, Japan) for providing us with *E. coli* tRNA transcripts.

Funding

Japan Society for the Promotion of Science [18H03980 and 23H00368 to K.T.]; Japan Science and Technology Agency [JPMJER2002 to T.S.]; Institute for Fermentation, Osaka (to K.T.); Takeda Science Foundation (to K.T.); Naito Foundation (to K.T.); Kobayashi Foundation (to K.T.). Funding for open access charge: Japan Society for the Promotion of Science (to K.T.).

Conflict of interest statement

None declared.

References

1. Goeders,N. and Van Melderen,L. (2014) Toxin–antitoxin systems as multilevel interaction systems. *Toxins*, **6**, 304–324.
2. Harms,A., Brodersen,D.E., Mitarai,N. and Gerdes,K. (2018) Toxins, targets, and triggers: an overview of toxin–antitoxin biology. *Mol. Cell*, **70**, 768–784.
3. Page,R. and Peti,W. (2016) Toxin–antitoxin systems in bacterial growth arrest and persistence. *Nat. Chem. Biol.*, **12**, 208–214.
4. Pandey,D.P. and Gerdes,K. (2005) Toxin–antitoxin loci are highly abundant in free-living but lost from host-associated prokaryotes. *Nucleic Acids Res.*, **33**, 966–976.
5. Gerdes,K., Bech,F.W., Jørgensen,S.T., Løbner-Olesen,A., Rasmussen,P.B., Atlung,T., Boe,L., Karlstrom,O., Molin,S. and von Meyenburg,K. (1986) Mechanism of postsegregational killing by the hok gene product of the parB system of plasmid R1 and its homology with the relF gene product of the *E. coli* relB operon. *EMBO J.*, **5**, 2023–2029.
6. Maisonneuve,E. and Gerdes,K. (2014) Molecular mechanisms underlying bacterial persisters. *Cell*, **157**, 539–548.
7. Yamaguchi,Y. and Inouye,M. (2011) Regulation of growth and death in *Escherichia coli* by toxin–antitoxin systems. *Nat. Rev. Microbiol.*, **9**, 779–790.

8. Hayes,F. and Van Melderen,L. (2011) Toxins–antitoxins: diversity, evolution and function. *Crit. Rev. Biochem. Mol. Biol.*, **46**, 386–408.
9. Wang,X., Yao,J., Sun,Y.C. and Wood,T.K. (2021) Type VII toxin/antitoxin classification system for antitoxins that enzymatically neutralize toxins. *Trends Microbiol.*, **29**, 388–393.
10. Jurėnas,D., Fraikin,N., Goormaghtigh,F. and Van Melderen,L. (2022) Biology and evolution of bacterial toxin–antitoxin systems. *Nat. Rev. Microbiol.*, **20**, 335–350.
11. Jia,X., Yao,J., Gao,Z., Liu,G., Dong,Y.H., Wang,X. and Zhang,H. (2018) Structure–function analyses reveal the molecular architecture and neutralization mechanism of a bacterial HEPN–MNT toxin–antitoxin system. *J. Biol. Chem.*, **293**, 6812–6823.
12. Yao,J., Zhen,X., Tang,K., Liu,T., Xu,X., Chen,Z., Guo,Y., Liu,X., Wood,T.K., Ouyang,S., *et al.* (2020) Novel polyadenylylation-dependent neutralization mechanism of the HEPN/MNT toxin/antitoxin system. *Nucleic Acids Res.*, **48**, 11054–11067.
13. Songailiene,I., Juozapaitis,J., Tamulaitiene,G., Ruksenaite,A., Šulčius,S., Sasnauskas,G., Venclovas,Č. and Siksnys,V. (2020) HEPN–MNT toxin–antitoxin system: the HEPN ribonuclease is neutralized by oligoAMPylation. *Mol. Cell*, **80**, 955–970.
14. Yu,X., Gao,X., Zhu,K., Yin,H., Mao,X., Wojdyla,J.A., Qin,B., Huang,H., Wang,M., Sun,Y.C., *et al.* (2020) Characterization of a toxin–antitoxin system in *Mycobacterium tuberculosis* suggests neutralization by phosphorylation as the antitoxicity mechanism. *Commun. Biol.*, **3**, 216.
15. Marimon,O., Teixeira,J.M., Cordeiro,T.N., Soo,V.W., Wood,T.L., Mayzel,M., Amata,I., García,J., Morera,A., Gay,M., *et al.* (2016) An oxygen-sensitive toxin–antitoxin system. *Nat. Commun.*, **7**, 13634.
16. Cai,Y., Usher,B., Gutierrez,C., Tolcan,A., Mansour,M., Fineran,P.C., Condon,C., Neyrolles,O., Genevaux,P. and Blower,T.R. (2020) A nucleotidyltransferase toxin inhibits growth of *Mycobacterium tuberculosis* through inactivation of tRNA acceptor stems. *Sci. Adv.*, **6**, eabb6651.
17. Xu,X., Usher,B., Gutierrez,C., Barriot,R., Arrowsmith,T.J., Han,X., Redder,P., Neyrolles,O., Blower,T.R. and Genevaux,P. (2023) MenT nucleotidyltransferase toxins extend tRNA acceptor stems and can be inhibited by asymmetrical antitoxin binding. *Nat. Commun.*, **14**, 4644.
18. Janowski,R., Panjikar,S., Eddine,A.N., Kaufmann,S.H. and Weiss,M.S. (2009) Structural analysis reveals DNA binding properties of Rv2827c, a hypothetical protein from *Mycobacterium tuberculosis*. *J. Struct. Funct. Genomics*, **10**, 137–150.
19. Wang,J., Yashiro,Y., Sakaguchi,Y., Suzuki,T. and Tomita,K. (2022) Mechanistic insights into tRNA cleavage by a contact-dependent growth inhibitor protein and translation factors. *Nucleic Acids Res.*, **50**, 4713–4731.
20. Hibi,K., Amikura,K., Sugiura,N., Masuda,K., Ohno,S., Yokogawa,T., Ueda,T. and Shimizu,Y. (2020) Reconstituted cell-free protein synthesis using *in vitro* transcribed tRNAs. *Commun. Biol.*, **3**, 350.
21. Walker,S.E. and Fredrick,K. (2008) Preparation and evaluation of acylated tRNAs. *Methods*, **44**, 81–86.
22. Zhang,C., Yashiro,Y., Sakaguchi,Y., Suzuki,T. and Tomita,K. (2020) Substrate specificities of *Escherichia coli* ItaT that acetylates aminoacyl-tRNAs. *Nucleic Acids Res.*, **48**, 7532–7544.
23. Yashiro,Y., Sakaguchi,Y., Suzuki,T. and Tomita,K. (2020) Mechanism of aminoacyl-tRNA acetylation by an aminoacyl-tRNA acetyltransferase AtaT from enterohemorrhagic *E. coli*. *Nat. Commun.*, **11**, 5438.
24. Nagao,A., Nakanishi,Y., Yamaguchi,Y., Mishina,Y., Karoji,M., Toya,T., Fujita,T., Iwasaki,S., Miyauchi,K., Sakaguchi,Y., *et al.* (2023) Quality control of protein synthesis in the early elongation stage. *Nat. Commun.*, **14**, 2704.
25. Yashiro,Y., Zhang,C., Sakaguchi,Y., Suzuki,T. and Tomita,K. (2021) Molecular basis of glycyl-tRNA^{Gly} acetylation by TacT from *Salmonella* Typhimurium. *Cell Rep.*, **37**, 110130.
26. Kabsch,W. (2010) XDS. *Acta Crystallogr. D Biol. Crystallogr.*, **66**, 125–132.
27. Afonine,P.V., Grosse-Kunstleve,R.W., Echols,N., Headd,J.J., Moriarty,N.W., Mustyakimov,M., Terwilliger,T.C., Urzhumtsev,A., Zwart,P.H. and Adams,P.D. (2012) Towards automated crystallographic structure refinement with phenix.refine. *Acta Crystallogr. D Biol. Crystallogr.*, **68**, 352–367.
28. Emsley,P., Lohkamp,B., Scott,W.G. and Cowtan,K. (2010) Features and development of Coot. *Acta Crystallogr. D Biol. Crystallogr.*, **66**, 486–501.
29. Toh,Y., Takeshita,D., Numata,T., Fukai,S., Nureki,O. and Tomita,K. (2009) Mechanism for the definition of elongation and termination by the class II CCA-adding enzyme. *EMBO J.*, **28**, 3353–3365.
30. Yamashita,S., Martinez,A. and Tomita,K. (2015) Measurement of acceptor–TΨC helix length of tRNA for terminal A76-addition by A-adding enzyme. *Structure*, **23**, 830–842.
31. Khlebnikov,A., Risa,O., Skaug,T., Carrier,T.A. and Keasling,J.D. (2000) Regulatable arabinose-inducible gene expression system with consistent control in all cells of a culture. *J. Bacteriol.*, **182**, 7029–7034.
32. Kinoshita,E., Kinoshita-Kikuta,E. and Koike,T. (2009) Separation and detection of large phosphoproteins using Phos-tag SDS–PAGE. *Nat. Protoc.*, **4**, 1513–1521.
33. Itoh,Y., Chiba,S., Sekine,S. and Yokoyama,S. (2009) Crystal structure of human selenocysteine tRNA. *Nucleic Acids Res.*, **37**, 6259–6268.
34. Li,F., Xiong,Y., Wang,J., Cho,H.D., Tomita,K., Weiner,A.M. and Steitz,T.A. (2002) Crystal structures of the *Bacillus stearothermophilus* CCA-adding enzyme and its complexes with ATP or CTP. *Cell*, **111**, 815–824.
35. Tomita,K., Fukai,S., Ishitani,R., Ueda,T., Takeuchi,N., Vassylyev,D.G. and Nureki,O. (2004) Structural basis for template-independent RNA polymerization. *Nature*, **430**, 700–704.
36. Tomita,K. and Yamashita,S. (2014) Molecular mechanisms of template-independent RNA polymerization by tRNA nucleotidyltransferases. *Front. Genet.*, **5**, 36.

Received: December 25, 2023. **Revised:** February 13, 2024. **Editorial Decision:** February 21, 2024. **Accepted:** February 28, 2024